Gas Temperature Structure of the Medium-Distant Galaxy Cluster Abell 1835 observed with XMM-Newton

T.H. REIPRICH
Max-Planck-Institut für extraterrestrische Physik, Postfach 1312, 85741 Garching, Germany; reiprich@mpe.mpg.de

Abell 1835 is the most distant galaxy cluster observed by XMM-Newton during the performance verification phase. The intracluster gas temperature profile of this massive cluster as observed with the EPIC-pn camera is presented. A clear temperature drop towards the center is detected. The temperature profile in the outer cluster parts is consistent with being flat. The complication of the temperature determination in the outer low surface brightness regions by various types of background, energy dependent vignetting, and out of time events is discussed.

1 Introduction

Knowledge about the temperature structure of the intracluster gas is vital for the determination of the gravitational cluster mass using the hydrostatic equation. The mass is the most fundamental cluster property and knowledge about the masses for a statistically complete sample of galaxy clusters can be used to put tight constraints on cosmological parameters [1]. Data from previous satellites has been used extensively in order to answer the question whether or not clusters show a trend of decreasing gas temperatures with increasing radius in the outer cluster parts in general [2,3,4,5]. The findings are contradictory. A significant temperature decrease would lead to an overestimate of total cluster masses if the gas is assumed to be isothermal. With the availability of cluster data obtained by XMM-Newton [6] it is now possible to determine the temperature profile accurately out to large physical radii. The large effective area, the good simultaneous spatial and spectral resolution combined with its field of view make XMM-Newton the ideal instrument to resolve the previous discrepancies.

Abell 1835 is an especially interesting galaxy cluster. First of all because of its medium redshift, $z = 0.252$. Only a few detailed temperature profiles for clusters around this redshift have been published up to now. Secondly A1835 is believed to host one of the most massive cooling flows with mass accretion rates $\dot{M} \sim 2\,000\,M_\odot\,\mathrm{yr}^{-1}$.[7] Following one of the major cluster specific XMM-Newton discoveries these mass accretion rates have been significantly reduced recently due to high resolution spectroscopy evidence obtained with the Reflection Grating Spectrometer (RGS) [8]. These facts make A1835 one of the crucial clusters to test the predictions of cooling flow and alternative models. Furthermore strong gravitational lensing has been observed [9] and the Sunyaev-Zeldovich effect has been measured for this cluster [10]. The latter measurement in combination with X-ray data has been used to constrain H_0 with the largest uncertainty being the uncertainty in the gas temperature available previously [10].

In this work the temperature profile of A1835 is determined from the central regions out to large radii utilizing data from the EPIC-pn camera [11] onboard XMM-Newton.

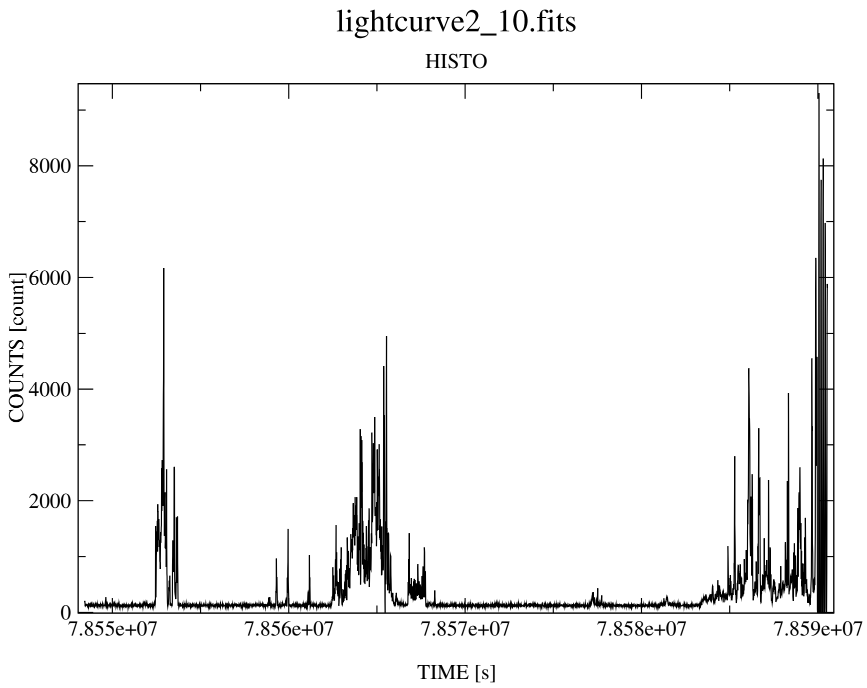

Figure 1: Lightcurve binned in 10 s intervals.

Throughout $H_0 = 50\,\mathrm{km\,s^{-1}\,Mpc^{-1}}$, $\Omega_\mathrm{m} = 1$, and $\Omega_\Lambda = 0$ is assumed.

2 Data Reduction and Analysis

Data taken with the Chandra and XMM-Newton observatories both suffer from times of very high background composed of 'soft protons'. In Fig. 1 the lightcurve of the EPIC-pn observation of A1835 is shown.[a] To obtain good statistics all events with energies above 0.3 keV have been selected. Most of the time the count rate, C_X, is stable at about 125 counts per 10 s. But occasionally huge flares are visible, reaching peak count rates more than 50 times higher than normal. Additionally smaller flares and times when the count rate drops to zero (counting mode times) appear. To increase the signal to noise ratio count rate thresholds ($100 \leq C_\mathrm{X} \leq 150$ counts per 10 s) for selection of good time intervals have been set after inspection of the count rate histogram (Fig. 2). The improvement is obvious in Fig. 3. Dozens of sources pop out of the background in the screened image. Since the four corners of the EPIC-pn camera are shielded against X-ray photons, the image on the right hand side in Fig. 3 also shows that most of the remaining background is Particle Induced Background (PIB; background induced directly or through instrumental lines by high energy particles).

For the spectral analysis all obvious point sources have been excluded as well as hot pixels and columns. Furthermore a correction has been applied to account for events counted during read out (out of time events, most obviously visible as the 'jet' extending from the cluster center parallel to the hot column, Fig. 3). The correction is done by creating an events file within the XMM SAS (Science Analysis System), where events have been redistributed randomly along columns keeping all other info, e.g., pattern and time[b]. The CTI (Charge Transfer Inefficiency) correction is done after the redistribution. Then a spectrum (or image) created from this events

[a]The events file has been created with SAS version xmmsas_20001220_1901.

[b]The time information in this events file is accurate up to one read out cycle.

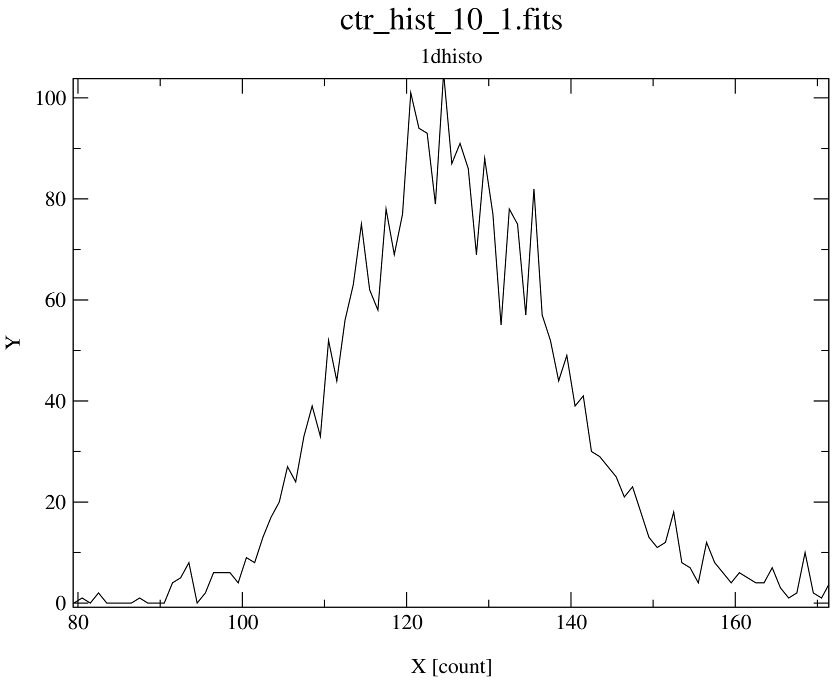

Figure 2: Central part of the count rate [counts per 10 s] distribution.

file is multiplied by a mode dependent factor (= 0.06 for Full Frame mode) and subtracted from the original spectrum (or image). Neglecting the influence of out of time events may lead to wrong temperature estimates since these events are assigned an incorrect CTI correction. Moreover, assume the cluster center has a lower temperature than the outer parts (as will actually be found later), then a spectrum taken from a ring of the outer low surface brightness region is contaminated by photons having a lower energy on average and the temperature estimate may be biased low.

The subtraction of the (remaining) background is performed using spectra created in the same way as outlined above. Various methods can be applied for background subtraction. The major drawbacks of two simple methods for the observation here are described as follows. One possibility is to use a 'blank sky' observation like the Lockman Hole observation and create a spectrum from the same detector region as the source spectrum, scaling by the source spectrum's exposure time. The disadvantage of this method is that it ignores variation in the Cosmic X-ray Background (CXB). The CXB is mainly composed of A) isotropic extragalactic emission (dominant for photon energies $E > 2\,\mathrm{keV}$) and B) anisotropic emission from galactic diffuse sources and 'hot bubbles' around the solar system (important for $E < 2\,\mathrm{keV}$). Galactic photoelectric absorption (important for $E < 1\,\mathrm{keV}$) causes an additional anisotropy. The CXB therefore can be considered as constant in time but varying with pointing direction (at soft energies) [12]. A further drawback is that a possible temporal variation of the normalization and/or spectrum of the PIB is ignored. Last not least if this method is used one must ensure that the flare filtering criteria are equivalent for science and background observation. This can be achieved, e.g., by assuming a constant PIB and selecting an energy band containing exclusively PIB and soft proton events (possibly $E > 12\,\mathrm{keV}$) with the drawback of a significant loss in statistics. Another simple method for the background subtraction is to use a ring outside the cluster emission in the science observation, taking advantage of the medium redshift of A1835 and XMM-Newton's field of view. Here the drawbacks are that the structure on the detector of the PIB is ignored. Using

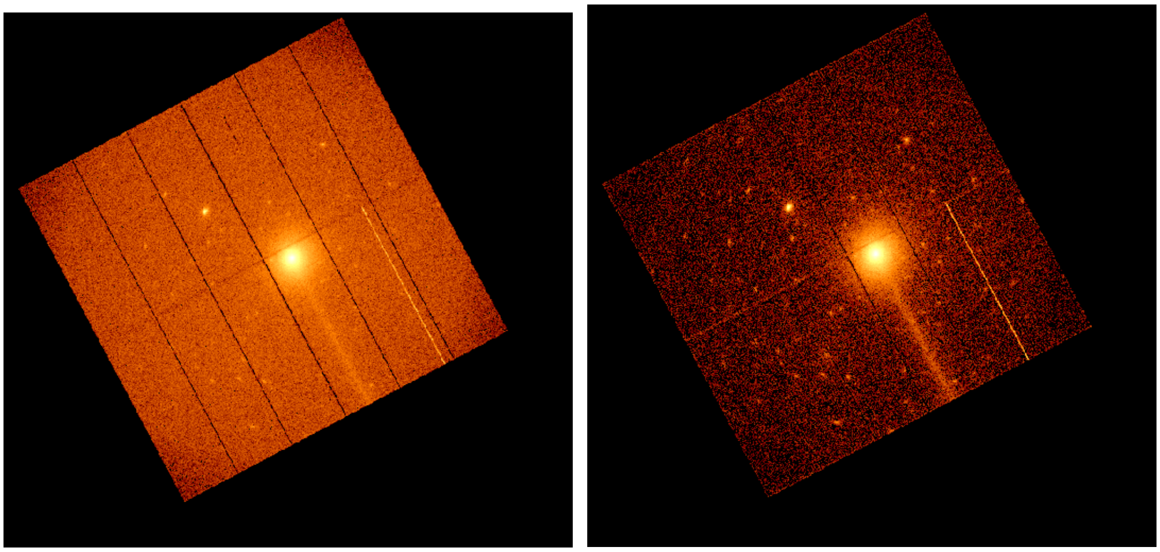

Figure 3: EPIC-pn images of A1835 in sky coordinates in the energy band 0.35–10 keV. The field of view is almost 30 arcmin. Left: Full 42 ks observation. Right: 25 ks good time intervals after application of the count rate thresholds.

this method also the question arises whether or not one should apply a vignetting correction for the background spectrum. If a correction is applied then the actually not vignetted PIB is overestimated. If no correction is applied then the vignetted CXB is underestimated.

More complicated methods are possible circumventing some of the above problems [13,14]. Here the background from not vignetting corrected data in a ring outside the cluster emission (7–11 arcmin from cluster center) has been taken because the PIB dominates the background. The main structural feature of the PIB is a fluorescent copper line at 8 keV, which is almost absent at the detector center but increases towards the outer parts of the EPIC-pn detector. Therefore events with $7.9 \leq E \leq 8.1$ keV have been excluded from the fit. With this method the CXB and PIB are corrected for in one step, since the CXB is not expected to change drastically for this small angular distance and variations in the PIB spectrum with time have no effect since exactly equivalent time intervals are used. Note, however, that the absolute contribution of the CXB is underestimated due to the vignetting increase with increasing radius. In the outer parts the fitted value of the column density of neutral hydrogen, $n_{\rm H}$, drops below the galactic value, which indicates that leaving $n_{\rm H}$ as a free parameter compensates for the underestimated CXB. However, the decrease of the $n_{\rm H}$ value is certainly not an ideal correction for this effect, since the spectral changes invoked by both effects probably do not cancel each other exactly. On the other hand using a vignetting corrected background for this method, where photons have been corrected individually, has resulted in worse fits and underestimated temperatures in the outer parts because of the wrongly corrected PIB. This is due to the dominance of the PIB at high energies and to the steeper vignetting increase with radius for higher energies.

Only singles, i.e., photons having deposited their energy in a single pixel on the CCD, have been selected for the spectral analysis. Most events are single events, but it is anticipated to include also double events and test the effects of a possible dependence of the single to double fraction on detector position in a future analysis. A 5-σ binning for the spectra has been used to ensure a significant signal in each bin. Choosing a 3-σ binning changes the fit results only well within the statistical errors. The energy range used has nominally been set to 0.3–10.0 keV. In the outer low surface brightness parts the number of significant high energy bins decreases. The fit parameter values have therefore been determined partly within smaller energy ranges. If two or more different temperatures are present for a specific radial bin then the availability of only

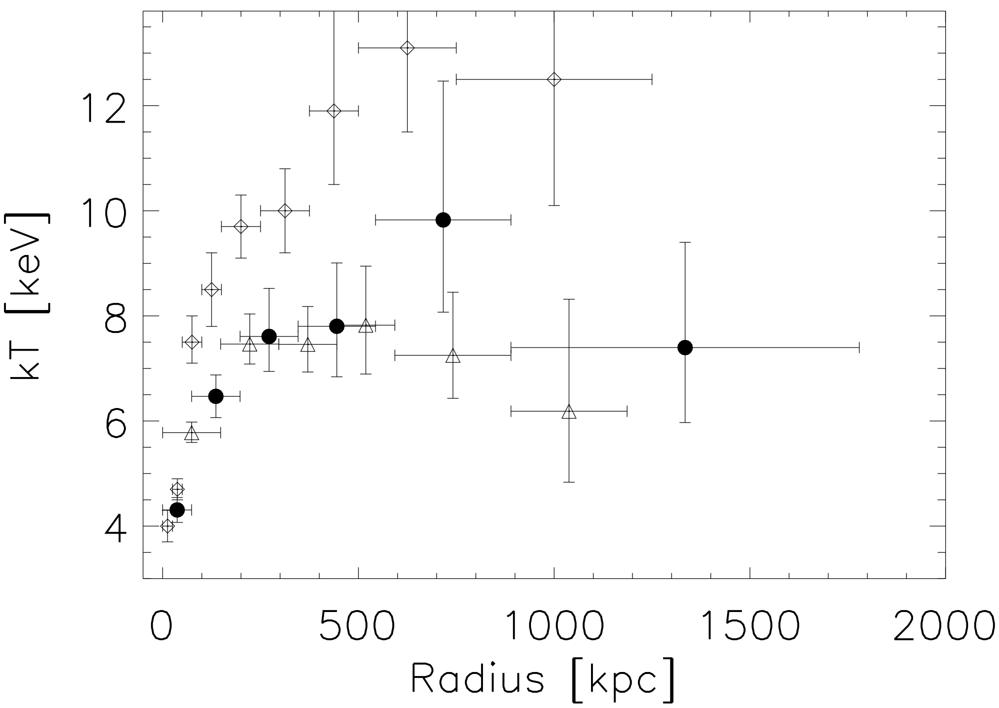

Figure 4: Temperature profiles as obtained with different detectors. Filled circles: EPIC-pn, this work; open triangles: EPIC-MOS2, Majerowicz & Neumann; open diamonds: Chandra, Schmidt, Allen, & Fabian. Vertical error bars indicate the 90 % confidence level statistical uncertainty for one interesting parameter for the first two works and the 1-σ statistical uncertainty for the last work. Horizontal bars indicate the radial bin size.

a weak signal at high energies may bias the estimated temperature in the outermost radial bin low. The presence of a lower signal to noise ratio at higher energies is independent of the binning method. The spectra have been modeled and fitted within XSPEC [15] using a single temperature MeKaL model including photoelectric absorption (wabs*mekal). The temperature, metal abundance, absorption column density, and normalization have been left as free parameters. Leaving the redshift as a free parameter yields values consistent with the optically determined redshift and with encouragingly small uncertainties. The 2001-05-07 release of EPIC-pn response matrices has been used. The spectra have not been deprojected, i.e., in the innermost radial bins also contributions from physically larger radii are included. However, the very steep radial surface brightness profile of A1835 ensures that these contaminating contributions are small. Changing the background normalization by $\pm 10\,\%$ has a negligible effect on the fit parameter values. Inclusion of arf files that correct the source spectra for telescope vignetting also affects the parameter values only insignificantly.

3 Results

The best fit cluster temperatures for six radial bins are shown in Fig. 4 as filled circles. The intracluster gas in the center ($R < 200\,\mathrm{kpc}$) is significantly cooler than in the outer parts, which may be caused either by a cooling flow [16] or by the Interstellar Medium (ISM) of the central brightest cluster galaxy [17]. Within the statistical uncertainty the temperature profile for $R > 200\,\mathrm{kpc}$ can be considered isothermal. Although at present a temperature decrease in the very outer part obviously cannot be excluded. The main limiting factor for a precise

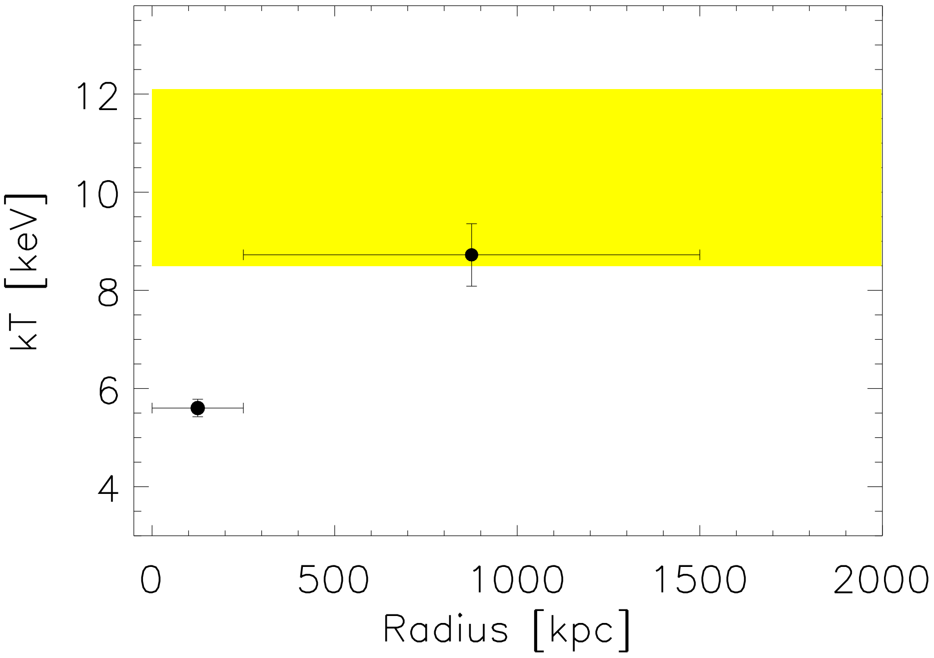

Figure 5: Overall gas temperature as estimated with EPIC-pn (upper filled circle; this work) and ASCA (shaded area; Allen et al.).

determination of the outer temperature is the relatively high PIB.

Also shown in Fig. 4 is the temperature profile determined using data from the EPIC-MOS2 camera onboard XMM-Newton by Majerowicz & Neumann [13] (open triangles). There is perfect agreement between the results from the two EPIC cameras out to $\sim 600\,\mathrm{kpc}$. For larger radii the temperature estimates are well consistent.

The open diamonds in Fig. 4 additionally indicate the temperature estimates obtained for A1835 with the Chandra satellite by Schmidt, Allen, & Fabian [18]. The agreement in the very center ($R < 100\,\mathrm{kpc}$) between the Chandra and EPIC-pn results is very good. For larger radii Chandra gives systematically higher temperatures, but note that 1-σ errors are shown for Chandra.

Using a two temperature model does not result in a significant improvement in any of the EPIC-pn fits, indicating the absence of evidence for gas with kT_{X} below $\sim 2\,\mathrm{keV}$. This is in agreement with the results obtained with the RGS [8].

To obtain a good estimate of the overall cluster temperature outside the central region a spectrum has been extracted within $250 \leq R \leq 1\,500\,\mathrm{kpc}$. The best fit temperature for this region $kT_{\mathrm{X}} = 8.7 \pm 0.6\,\mathrm{keV}$ (90 % c.l.). In Fig. 5 this result is compared to the previous estimate from ASCA (shaded area; Allen et al. [7]). The ASCA data suggest a higher temperature but the results are consistent. Note that the errors have been decreased significantly with EPIC-pn.

Comparing this overall cluster temperature and A1835's X-ray luminosity as measured with a ROSAT PSPC pointed observation with the L_{X}–T_{X} relation of a local sample one finds that within the scatter it falls nicely onto this relation (Fig. 6). Moreover the exceptionally strong central cool emission in A1835 may boost the total X-ray luminosity, which would explain the slightly higher luminosity than expected from the relation.

The metal abundance profile relative to solar abundances [19] is found to be flat within the statistical errors (Fig. 7). The mean abundance is about 0.35 solar.

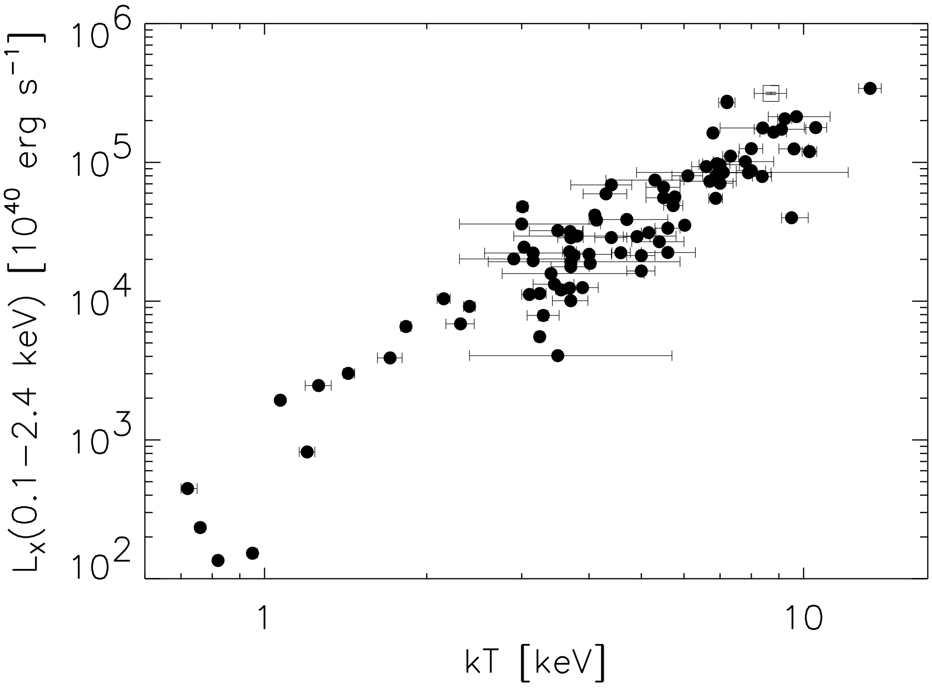

Figure 6: Luminosity and temperature of A1835 (open square) as compared to the L_X–T_X relation of a local sample (88 clusters compiled during construction of *HIFLUGCS*; Reiprich & Böhringer 2001).

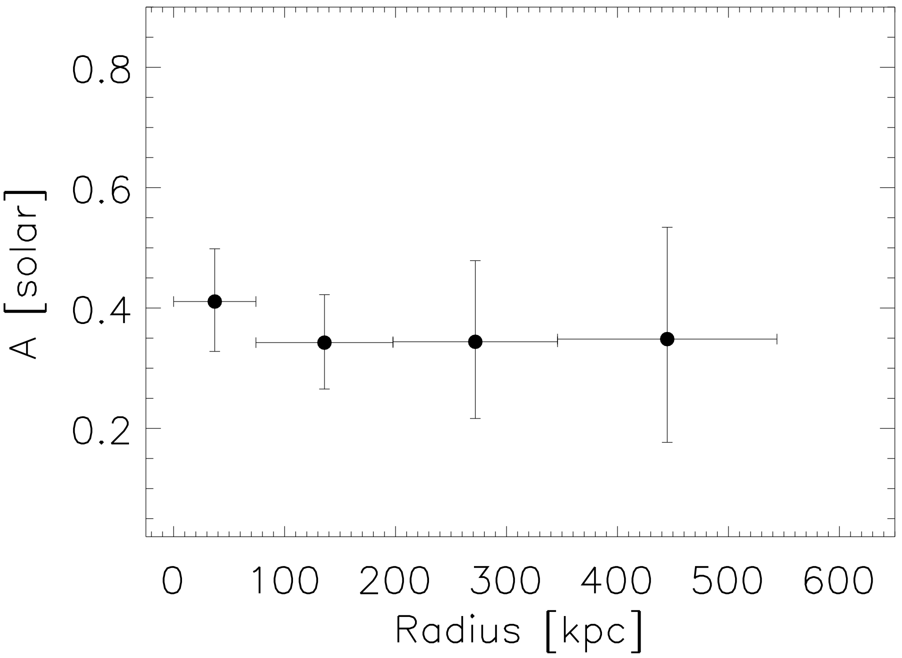

Figure 7: Metal abundance profile as determined with the EPIC-pn camera.

4 Conclusions

The intracluster gas in the central region is significantly cooler than in the outer part of A1835. The gas in the outer part is consistent with being isothermal.
No indications for gas temperatures below $\sim 2\,\mathrm{keV}$ have been found.
The metal abundance profile is consistent with being flat.
The cluster temperature within $250 \leq R \leq 1\,500\,\mathrm{kpc}$ has been determined as $kT_{\mathrm{X}} = 8.7 \pm 0.6$. This significantly reduced error on the overall cluster temperature allows to put tighter constraints on H_0 in combination with the SZ effect.
Assuming the cluster temperature to stay isothermal beyond $1\,500\,\mathrm{kpc}$ an estimate of the total gravitational mass has been obtained utilizing the gas density profile determined from a ROSAT PSPC pointed observation. Under the assumption of hydrostatic equilibrium it is found that $M_{\mathrm{tot}} = 1.3 \pm 0.2 \times 10^{15}\,M_{\odot}$ within $R_{500} = 2.1\,\mathrm{Mpc}$.
Future work including also double events will allow to tighten the constraints on the temperature estimates.
This article is available electronically at: http://www.xray.mpe.mpg.de/~reiprich/act/publi.html

Acknowledgements

This work is based on observations obtained with XMM-Newton, an ESA science mission with instruments and contributions directly funded by ESA Member States and the USA (NASA). The author acknowledges the benefit from discussions with the XMM-Newton hardware and software teams at MPE. I would like to thank Sébastien Majerowicz at CEA-Saclay for valuable discussions as well as Yasushi Ikebe, Kyoko Matsushita, Alexis Finoguenov, and Hans Böhringer at MPE. Manami Sasaki has provided software to correct individual photons for vignetting. Robert Schmidt has kindly made available the Chandra results prior to publication. Last not least I would like to thank Doris Neumann and co-organizers for the realization of this enjoyable meeting.

References

1. T. H. Reiprich and H. Böhringer. *ApJ, submitted*, 2001.
2. M. Markevitch, W. R. Forman, C. L. Sarazin, and A. Vikhlinin. *ApJ*, 503:77–96, August 1998.
3. J. A. Irwin, J. N. Bregman, and A. E. Evrard. *ApJ*, 519:518–532, July 1999.
4. D. A. White. *MNRAS*, 312:663–688, March 2000.
5. J. A. Irwin and J. N. Bregman. *ApJ*, 538:543–554, August 2000.
6. F. Jansen, D. Lumb, B. Altieri, J. Clavel, M. Ehle, C. Erd, C. Gabriel, M. Guainazzi, P. Gondoin, R. Much, R. Munoz, M. Santos, N. Schartel, D. Texier, and G. Vacanti. *A&A*, 365:L1–L6, January 2001.
7. S. W. Allen, A. C. Fabian, A. C. Edge, M. W. Bautz, A. Furuzawa, and Y. Tawara. *MNRAS*, 283:263–281, November 1996.
8. J. R. Peterson, F. B. S. Paerels, J. S. Kaastra, M. Arnaud, T. H. Reiprich, A. C. Fabian, R. F. Mushotzky, J. G. Jernigan, and I. Sakelliou. *A&A*, 365:L104–L109, January 2001.
9. S. W. Allen. *MNRAS*, 296:392–406, May 1998.
10. P. D. Mauskopf, P. A. R. Ade, S. W. Allen, S. E. Church, A. C. Edge, K. M. Ganga, W. L. Holzapfel, A. E. Lange, B. K. Rownd, B. J. Philhour, and M. C. Runyan. *ApJ*, 538:505–516, August 2000.
11. L. Strüder, U. Briel, K. Dennerl, R. Hartmann, E. Kendziorra, N. Meidinger, E. Pfeffermann, C. Reppin, B. Aschenbach, W. Bornemann, H. Bräuninger, W. Burkert, M. Elender,

M. Freyberg, F. Haberl, G. Hartner, F. Heuschmann, H. Hippmann, E. Kastelic, S. Kemmer, G. Kettenring, W. Kink, N. Krause, S. Müller, A. Oppitz, W. Pietsch, M. Popp, P. Predehl, A. Read, K. H. Stephan, D. Stötter, J. Trümper, P. Holl, J. Kemmer, H. Soltau, R. Stötter, U. Weber, U. Weichert, C. von Zanthier, D. Carathanassis, G. Lutz, R. H. Richter, P. Solc, H. Böttcher, M. Kuster, R. Staubert, A. Abbey, A. Holland, M. Turner, M. Balasini, G. F. Bignami, N. La Palombara, G. Villa, W. Buttler, F. Gianini, R. Lainé, D. Lumb, and P. Dhez. *A&A*, 365:L18–L26, January 2001.
12. Y. Ishisaki. PhD thesis, Univ. Tokyo, 1997.
13. S. Majerowicz and D. Neumann. *These proceedings*, 2001.
14. G. W. Pratt, M. Arnaud, and N. Aghanim. *These proceedings*, 2001.
15. K. A. Arnaud. In *ASP Conf. Ser. 101: Astronomical Data Analysis Software and Systems V*, volume 5, pages 17–20, 1996.
16. A. C. Fabian. *ARA&A*, 32:277–318, 1994.
17. K. Makishima, H. Ezawa, Y. Fukazawa, H. Honda, Y. Ikebe, T. Kamae, K. Kikuchi, K. Matsushita, K. Nakazawa, T. Ohashi, T. Takahashi, T. Tamura, and H. Xu. *PASJ, accepted. Preprint: astro-ph/0104079*, 2001.
18. R. Schmidt, S. W. Allen, and A. C. Fabian. *MNRAS, submitted*, 2001.
19. E. Anders and N. Grevesse. *Geochim. Cosmochim. Acta*, 53:197–214, January 1989.